# INFLUENCE OF BEAM JITTER ON THERMAL BLOOMING

Frederick G. Gebhardt

United Technologies Research Center

Prepared for:

Naval Research Laboratory
Advanced Research Projects Agency

1 August 1975

# Influence of Beam Jitter on Thermal Blooming



**Semi-Annual Technical Report**

**August 1,1975**

**Period covered: January 6,1975 to June 30,1975**

**Sponsored By**

**Advanced Research Projects Agency**

**ARPA Order No. 2439**

**CONTRACT No. N00014-75-C-0649**

**F.G. Gebhardt**

SECURITY CLASSIFICATION OF THIS PAGE (When Data Entered)

# REPORT DOCUMENTATION PAGE

READ INSTRUCTIONS BEFORE COMPLETING FORM

| | |
|---|---|
| 1. REPORT NUMBER: R75-922050-6 | 2. GOVT ACCESSION NO. |
| 3. RECIPIENT'S CATALOG NUMBER | |
| 4. TITLE (and Subtitle): Influence of Beam Jitter on Thermal Blooming | 5. TYPE OF REPORT & PERIOD COVERED: Jan. 1, 1975 - June 30, 1975 Semi-Annual Tech. Repor |
| 6. PERFORMING ORG. REPORT NUMBER: R75-922050-6 | |
| 7. AUTHOR(s): Frederick G. Gebhardt | 8. CONTRACT OR GRANT NUMBER(s): N00014-75-C-0649 |
| 9. PERFORMING ORGANIZATION NAME AND ADDRESS: United Technologies Research Center, 400 Main Street, East Hartford, CT 06108 | 10. PROGRAM ELEMENT, PROJECT, TASK AREA & WORK UNIT NUMBERS: ARPA |
| 11. CONTROLLING OFFICE NAME AND ADDRESS: Defense Advanced Research Projects Agency, 1400 Wilson Boulevard, Arlington, VA 22209 | 12. REPORT DATE: August 1, 1975 |
| | 13. NUMBER OF PAGES: 44 |
| 14. MONITORING AGENCY NAME & ADDRESS (if different from Controlling Office): Naval Research Laboratory, 4555 Overlook Avenue, S. W., Washington, D. C. 20375 | 15. SECURITY CLASS. (of this report): Unclassified |
| | 15a. DECLASSIFICATION/DOWNGRADING SCHEDULE |

16. DISTRIBUTION STATEMENT (of this Report)

17. DISTRIBUTION STATEMENT (of the abstract entered in Block 20, if different from Report)

18. SUPPLEMENTARY NOTES

19. KEY WORDS (Continue on reverse side if necessary and identify by block number)

Laser Beam Jitter
Thermal Blooming
High Power Propagation
Atmospheric Simulation

20. ABSTRACT (Continue on reverse side if necessary and identify by block number)

Laboratory simulation experiments have been carried out to investigate the effects of beam jitter on the thermal blooming of a laser beam propagating in an absorbing medium with a transverse wind. Results obtained with a broadband, low pass white noise jitter frequency spectrum are in good agreement with the root-sum-square approach which considers the jitter and blooming effects to be independent. The effects of beam jitter on the scaling laws for thermal blooming are considered.

DD FORM 1 JAN 73 1473 EDITION OF 1 NOV 65 IS OBSOLETE

SECURITY CLASSIFICATION OF THIS PAGE (When Data Entered)

UNITED TECHNOLOGIES RESEARCH CENTER

Report Number: R75-922050-6
Semi-Annual Technical Report for the Period
6 January 1975 to 30 June 1975

Influence Of Beam Jitter On
Thermal Blooming

| | |
|---|---|
| ARPA Order No.: | 2439 |
| Program Code No.: | Z45000 |
| Contractor: | United Technologies Research Center |
| Effective Date of Contract: | January 6, 1975 |
| Contract Expiration Date: | March 5, 1976 |
| Amount of Contract: | $69,262 |
| Contract No.: | N00014-75-C-0649 |
| Principal Investigator: | Dr. David C. Smith (203) 565-5281 |
| Scientific Officer: | Director, Naval Research Laboratory (Code 5560) 4555 Overlook Avenue, S.W. Washington, D.C. 20375 |
| Short Title: | Jitter and Thermal Blooming |
| Report By: | Dr. F.G. Gebhardt (203) 565-7006 |



Sponsored By
Advanced Research Projects Agency
ARPA Order No. 2439

TABLE OF CONTENTS

Technical Report

## SUMMARY

Under this contract, the influence of beam jitter on the thermal blooming of a laser beam is being investigated. Thermal blooming is the self-induced thermal distortion of a laser beam caused by the absorption of a portion of the laser beam energy which heats the air in the path of the beam and, in turn, results in changes of the refractive index that produce the beam distortion. With a stationary or uniformly slewing cw laser beam propagating in the atmosphere with a uniform transverse wind the thermal distortion effects reach a steady-state during the wind transit time across the beam. The blooming effects under these conditions have been studied extensively and are now well understood. In practical situations, however, there is beam wander or motion due to jitter of the pointer/tracker telescope or atmospheric turbulence which introduces transient effects that greatly complicate the analysis and lead to the requirement for complex 4-D computer code calculations. Therefore, the purpose of this program is to examine experimentally and theoretically the interaction of beam jitter and thermal blooming with the objective of improving the understanding and ability to model high power laser beams propagation in the atmosphere. The approach used is to examine the jitter effects on blooming using scaled laboratory experiments to simulate the conditions anticipated in realistic Navy scenarios.

In this report the progress made during the first six months of the program is described. Briefly, an experimental thermal blooming facility has been assembled with a 40 W $CO_2$ laser, attenuator and a telescope to focus the beam through an enclosed recirculating wind tunnel with an absorbing gas to simulate a transverse wind in the atmosphere. A pair of electrically driven orthogonally mounted, galvonometer mirror scanners are used to produce the beam jitter at the entrance window of the absorbing path. Two independent, white noise sources are used to produce independent zero mean equal variance random x-y jitter signals to simulate the symmetric long-time average spreading due to telescope tracking jitter. The frequency dependence of the jitter effects on blooming is examined by controlling the jitter drive signal spectrum with either low-pass broadband or tunable narrow bandpass filters. Experimental results obtained to date have been with broadband, low-pass ( $\approx$ 0-150Hz) jitter signals and a characteristic blooming frequency of $\approx$40 Hz is defined by the wind tunnel velocity divided by the focused beam diameter. The relative irradiance with both beam jitter and thermal blooming is found to correlate well with estimates based on the root-sum-square (RSS) hypothesis, which implies negligible interaction between the jitter and blooming processes. In addition, the critical (or optimum) irradiance and power levels respectively, decrease and increase with increasing beam jitter as expected on the basis of simple scaling laws.

In the remaining portion of the program additional experimental results for jitter effects on blooming will be obtained with particular emphasis on the frequency dependence and its influence on modeling the effects.

# I. INTRODUCTION

The self-induced thermal distortion of laser beams in the atmosphere is a serious problem for high power laser applications and has received considerable attention both experimentally (Ref. 1-6) and theoretically (Ref. 3, 7-10). In these previous studies of thermal blooming effects on cw beams the emphasis has been primarily on the idealized case of the steady-state thermal distortion that occurs with a uniform wind field along the beam path or, in addition, with beam slewing. In practical applications, the situation actually is more complex since transient effects due to the scintillation and beam wander associated with atmospheric turbulence and the jitter of the transmitter optics are also encountered. To analyze theoretically the influence of these and other transient effects on the thermal blooming is difficult and requires the use of a complex four-dimensional computer code (Ref. 11). Another approach, which is relatively straightforward and thus, may be simpler is to examine the effects experimentally and use the results to verify the 4-D code calculations as well as to determine empirically the appropriate changes to the scaling laws for cw thermal blooming. Thus, in the present program, being conducted by UTRC for the U.S. Navy under the sponsorship of the Defense Advanced Research Projects Agency, an experimental and theoretical investigation of the effects of beam jitter on cw thermal blooming is being carried out. The purpose of the program is to examine in laboratory simulation experiments for conditions of interest to the Navy the interaction of beam jitter effects on thermal blooming and through simplified theoretical analyses attempt to model the experimental results and develope procedures to account for beam jitter effects on the scaling laws for cw thermal blooming.

The progress made during the first six months of the subject program is described in this semi-annual technical report. In Section II some basic considerations of laser beam jitter are discussed to help in defining the requirements of the laboratory simulation experiments. The experimental arrangement and procedure for examining the influence of beam jitter effects on thermal blooming is described in Section III. Section IV contains the experimental results obtained to date for the interaction of wide-band (DC-250 Hz) beam jitter with thermal blooming. In Section V the root-sum-square approach to modeling beam jitter effects on blooming is discussed and used to obtain modified scaling laws for the critical or optimum irradiance and power. Finally, plans for conducting further beam jitter and blooming experiments with tunable narrow-band noise at frequencies below, comparable to and above the characteristic blooming frequency are described in Section VI.

## II. LASER BEAM JITTER

Laser beam jitter can result from a variety of sources within the laser system and is a serious limitation on the pointing accuracy of the beam. For example, beam jitter may be due to instabilities in the laser medium, vibrations in the cavity optics, optical train or laser platform or from the residual noise or hunting instabilities of the pointing and tracking system for the primary transmitter mirror. It is not the purpose of this discussion to point out all the possible sources of jitter but, rather, to estimate the magnitude and frequency spectra of the jitter that may be expected for realistic naval scenarios and to consider qualitatively its effect on thermal blooming.

The rms magnitude and frequency spectrum of beam jitter will, of course, depend on the details of the laser platform and vehicle design. Typically a servo controlled stabilizing platform is used to reduce the gross motion and vibrations transferred from the vehicle to the pointing mirror. Also servo controlled autoalignment and pointer/tracker systems may be employed for the laser/optical train and telescope, respectively. In any case, system noise and errors will always result in a certain residual level of beam jitter which, based on current state-of-the-art systems, corresponds to rms jitter angles in the range of 10 μradians or greater with frequencies in the range of 0.5 to 80 Hz (Ref. 12). A typical example for the power spectrum of jitter which a laser beam may experience is shown in Fig. 1. In addition to the low frequency peak below 1 Hz there is a second peak around 30 Hz. At higher frequencies the jitter spectrum falls off at a rate of about 25 dB/decade. For the example in Fig. 1, the rms jitter is $\theta_J = 15\mu$ radians as found by integrating the spectrum to obtain the mean square beam jitter $\theta_J^2$.

The effect of beam jitter on linear propagation is to tend to reduce the time-average peak irradiance at the target. In particular for a randomly wandering Gaussian beam, the average irradiance distribution can be shown to also be Gaussian with the 1/e beam radius increased by the factor $(1 + \theta_J^2/\theta_o^2)^{1/2}$, where $\theta_J$ is the rms jitter angle and $\theta_o = 1/ka_o$ is the diffraction spreading angle of the Gaussian beam with $a_o$ equal to the 1/e radius at the source and $k = 2\pi/\lambda$ is the wavenumber with $\lambda$ the wavelength. Here we have assumed the orthogonal jitter angles $\theta_x$, $\theta_y$ to be independent and normally distributed random variables with zero means and equal variances $\bar{\theta}_x^2 = \bar{\theta}_y^2 = \theta_J^2/2$, i.e., the jitter is isotropic. Clearly, the beam jitter has a significant effect on the average irradiance only if $\theta_J/\theta_o \gtrsim 1$, or, if the aperture diameter $D = 2\sqrt{2}\,a_o \gtrsim \lambda/2\,\theta_J$. Thus, for the example in Fig. 1 with $\theta_J = 15\mu$ radians, the effects of jitter become important for aperture diameters $D \gtrsim 13$ cm and 35 cm for $\lambda = 3.8\mu$m and 10.6 μm, respectively.

The interaction of beam jitter with thermal blooming introduces a transient aspect to the problem since the beam position at a fixed range is wandering randomly about the pointing axis. The convective thermal blooming effects depend on the re-

moval of absorbed energy by the motion of the air relative to the beam. Assuming the mean relative air velocity resulting from both wind and beam slewing is $v(z)$ and the beam diameter is $d(z)$, the characteristic blooming time $t_B(z) = d(z)/v(z)$ is required for the steady-state convective thermal lens to be established at the particular range z. The effects of beam jitter on the thermal blooming can be simply understood in the two limiting, idealized cases where the characteristic jitter frequency $f_J$ is either very large or very small compared to the characteristic "blooming" frequency $f_B(z) \approx 1/t_B(z)$. Thus, when the jitter motion is very rapid, i.e., $f_J/f_B >> 1$, the steady-state blooming and the average irradiance can be predicted based on the average irradiance profile with only jitter effects included. For the case of very slow jitter motion, i.e., $f_J/f_B << 1$, the blooming can be predicted based on the irradiance profile without jitter and the average irradiance is found by averaging over the jitter motion of the bloomed irradiance distribution. In these two limiting cases the effects of jitter or beam wander and blooming are uncoupled and treated independently by virtue of the averaging process.

When the jitter and blooming frequencies are comparable it is no longer obvious that the effects can be decoupled and treated separately. In general, the situation is also complicated by the fact that the blooming frequency varies along the path due to focusing and slewing and, in addition, the jitter motion consists of a spectrum of frequencies rather than a single characteristic frequency.

To give an example, consider the following case:

$\lambda = 3.8\mu m$

$D = 50$ cm

$z = 3$ km

$v = 10$ m/sec

$d(3km) = 2.9$ cm

Here, the blooming frequency varies over the range, $20 \lesssim f_B \lesssim 350$ Hz, in going from the source aperture to the focal plane. Except near the aperture where the jitter motion is small anyway the jitter frequencies shown in Fig. 1 tend to be smaller than the blooming frequencies, i.e., $f_J/f_B \lesssim 1$, in this case. Smaller crosswind velocities, larger aperture diameters and longer ranges would all tend to reduce the blooming frequencies and increase the amount of overlap with the jitter frequency spectrum.

The beam wander effects associated with atmospheric turbulence should be essentially the same as jitter with regard to their effects on thermal blooming. In this case the characteristic beam wander frequencies should be comparable to the blooming frequency near the source aperture since the index gradients in this region are most

important in producing the wander effects. In the experimental program to investigate the beam jitter effects on thermal blooming the jitter frequency spectrum will be one of the variables and the various extremes of $f_J/f_B <, \approx, > 1$ will be examined. From the preceding discussion it appears, however, that in most practical situations with focused beams and slewing the condition $f_J/f_B \lesssim 1$ holds over most of the path.

## III. EXPERIMENTAL FACILITY

In this section the equipment, experimental arrangement and types of beam jitter signals used to investigate beam jitter effects on thermal blooming will be described.

The basic experimental arrangement for examining beam jitter effects on thermal blooming is shown in Fig. 2. The principal equipment components consist of (1) the laser, attenuator and telescope; (2) device to produce beam jitter; (3) recirculating, enclosed wind tunnel containing absorbing gas to simulate the effect of a transverse wind; and (4) diagnostic equipment including power meters, variable aperture & point detectors and Kalvar film. With the exception of the beam jitter apparatus all of the equipment was available from previous thermal blooming studies. Extensive modifications and testing of the wind tunnel were required, however, to obtain a stable, low velocity flow and also reduce the boundary layer thickness at the entrance window to the absorbing path. Basically, the changes involved replacing the original six 200 cfm blowers with a single 30 cfm blower, increasing the area ratio between the optical path test section and input side of the two-dimensional venturi and the installation of new window mounts which place the inner surface away from the end wall to reduce boundary layer effects. Also a variety of foam pieces with different thicknesses and porocity were tested to improve flow uniformity and stability. The best configuration for uniform and stable low velocity flow was found, however, to be with no foam at all and only a 0.5 in square mesh by 0.5 in thick fluorescent light diffuser used as a flow straightener before the test section venturi. The wind tunnel flow has been probed at five positions, each spaced approximately 24 cm apart, along the 1m optical path, with a hot wire anemometer (Flow Corporation Series 800 Flowmeter). The flow was found to be stable and uniform at the five test positions along the optical path over the available velocity range estimated to be from a minimum of 1-5 cm/sec to a maximum of 15-20 cm/sec. (Ref. 13).

Because of the operation of the wind tunnel at 1 atm pressure as opposed to near 10 atm in most of the previous blooming studies involving gases in a translating absorption cell, (Ref. 4) a larger velocity is required to prevent conduction effects from interfering with the simulation of the convection dominated thermal blooming which is important in the atmosphere. The higher velocity which is also dictated by requirements for the uniformity and stability of the wind tunnel flow, means that more laser power is required to obtain the same amount of thermal distortion for the same beam geometry and fractional absorption. Thus, a second gain tube has been added to the existing $CO_2$ laser to increase the output power capability from 15-20W to greater than 40W for single ($TEM_{oo}$) mode operation.

The experimental arrangement and basic procedures used to observe the thermal distortion effects has been described in detail previously (Ref. 4, 14). The main difference between these experiments with the recirculating wind tunnel and those conducted with the moving cell is that the thermal distortion effects can be observed indefinitely rather than only the several seconds duration allowed by the 4.5 cm cell diameter. The continuous thermal distortion effects provided by the recirculating wind tunnel allows much longer averaging times to be employed and also simplifies the required beam diagnostics relative to the moving cell approach.

To provide beam jitter in the experiments two orthogonally mounted, electronically driven galvonometer scanner mirrors are employed. The mirror scanners (General Scanning G-300 PD) include position detectors with closed loop servo control and drive electronics to avoid mechanical resonance problems and provide a flat frequency response. The frequency response as measured with a focused HeNe laser beam is shown in Fig. 3 for both the horizontal (parallel to wind tunnel flow) and vertical mirror scanners. The response of both scanners is flat to within $\pm$ 0.8 dB from 5 to 100 Hz and at higher frequencies rolls off at a rate of 3 dB per octave.

In determining the type of jitter drive signals to be used to simulate the beam motion of a typical pointer/tracker telescope single frequency sinusoidal signals were considered initially. Although single frequency sinusoidal jitter motion is convenient and desirable for studying the dependence of the jitter effects on blooming on the ratio of jitter-to-blooming frequency, $f_J/f_B$, the resulting beam motion at the focal plane is in the form of a lissajous pattern that varies from a diagonal line to an ellipse or circle depending on the relative amplitudes and phases of the x-y drive signals. In addition, a single frequency sinusoidal one-dimensional jitter, which has been considered as an interesting choice for its analytical convenience, tends to produce a bimodal spreading of the average irradiance profile. Since, lacking more specific information, it is more reasonable to assume that typically pointer/tracker beam jitter results in an isotropic spreading of the average beam pattern to a circular shape with a central peak, because of its origin in zero-mean, random noise signals, the single frequency sinusoidal jitter signals with beam motion, as described above, does not appear to be the best choice for the simulation experiments. Thus, we have chosen instead to use two independent thermal noise signals to provide the x-y beam jitter in the simulation experiments. A block diagram of the jitter signal drive electronics for the horizontal scanner is shown in Fig. 4. Broadband noise from DC to 300 Hz is generated by a high-gain differential amplifier (Tektronix 1A7A). This noise signal is then fed into either a broadband low-pass amplifier or a tunable bandpass filter (Tektronix AF501) to provide either a broadband (0-300 Hz)

or tunable (3Hz-300 Hz) narrow band (effective Q-15) random noise signal to drive the galvonometer scanner. For the horizontal scanner channel, as shown, a slow rampsweep signal can be added to the noise to slowly scan the jittered beam across a point detector for recording the time average irradiance profile. An rms reading voltmeter is used to measure and calibrate the random noise signals for both the x and y scanner channels.

## IV. EXPERIMENTAL RESULTS

In this section, we present the experimental results obtained to date for the effects of beam jitter on thermal blooming.

In all of the experiments to be discussed, the jitter drive signals used were wideband (0-300 Hz) random noise, with the jitter motion modified by the scanner response (i.e., 3 dB bandwidth is from < 5 Hz to 250 Hz) as shown in Fig. 2. Data are shown for experiments conducted on three dates: 4/11, 4/23 and 4/24. The experimental parameters are given in Table I. The absorbing gas used in the wind tunnel is nitrogen-seeded with a small amount of propylene ($C_3H_6$) at a total pressure of one atmosphere. The wind tunnel is equipped with 5 cm diameter, 0.6 cm thick NaCl windows. For all but the 4/24 data the beam distortion measurements were made using a variable aperture centered on the average peak irradiance to provide a cumulative power distribution curve, i.e., the fraction of the total power collected as a function of increasing aperture diameter. The position of the peak of the average irradiance profile was found by manually scanning the small aperture along the flow direction through beam center. The 4/24 measurements, however, were made with the beam slowly scanned across a fast point detector and the average irradiance profile is obtained from an oscilloscope trace.

The irradiance profile and a Kalvar film image of the laser beam at the wind tunnel entrance window is shown in Fig. 5 for the data obtained on 4/11. The beam shape is nonsymmetrical and deviates substantially from a Gaussian profile presumably because of a slight misalignment of the laser cavity or degradation of the NaCl Brewster angle windows.

The irradiance profiles and Kalvar film images of the unbloomed focal spot are shown in Fig. 6 both without and with beam jitter. The jitter drive signal level was adjusted to be 3 millivolts rms at the input to the scanner drive amplifier (see Fig. 4). This amount of jitter reduces the mean on-axis irradiance level to about 43% of the value wihtout jitter and thus corresponds to an rms radial motion of the focal spot of 1.15 times the undistorted beam radius. Taking d = 0.2 cm as the diameter of the undistorted spot and with the wind tunnel velocity v = 8 cm/sec, the blooming frequency at focus is $f_B \sim 40$ Hz. Since much of the jitter energy lies at higher frequencies, i.e., $f_J/f_B > 1$ for most of the jitter motion, the blooming effects should be expected to correlate with the blooming predicted on the basis of the average unbloomed beam profile including jitter. That is to say, the characteristic blooming time is sufficiently long to average over most of the random jitter induced beam motion.

In Figs. 7 and 8, cumulative power distribution curves are shown with and without the beam jitter (rms level $a_J/a_o = 1.15$) for weak and strong blooming conditions, respectively. The results without thermal blooming are indicated by the open symbols

and the circles and triangles represent the cases without and with beam jitter, respectively. The weak and strong blooming cases refer to the power levels of $P_{in}$ = 5.5 W and 11 W for which the values of the distortion parameter are N = 2.9 and 5.9, respectively (Ref. 4).

The results of the jitter and blooming experiments have been analyzed using the aperture diameter $d_e$ containing 63% of the total power to define an effective beam area, $A = \pi d_e^2/4$. Thus, we define the relative irradiance $I_{REL} = A_o/A = (d_{eo}/d_e)^2$, where $A_o$ and A (or, $d_{eo}$ and $d_e$) refer to the effective area (or diameters) of the ideal (i.e., unjittered and unbloomed) and distorted beams, respectively. The values for $I_{REL}$ obtained from the 4/11 data in Figs. 7 and 8 are shown in Table II. For the weak blooming case (N = 2.9), the values $I_{REL}$ = 0.46 and 0.32 were obtained without and with the beam jitter, respectively. For the strong blooming case (N = 5.9), the values $I_{REL}$ = 0.094 and 0.096 were obtained without and with beam jitter, respectively.

The value of $I_{REL}$ can be estimated on the basis of the simple addition of areas $A = A_o + A_B + A_J$, where $A_B$ and $A_J$ are determined from the relations

$$I_{REL}(B) = \frac{1}{1 + A_B/A_o} \qquad (4\text{-}1)$$

$$I_{REL}(J) = \frac{1}{1 + A_J/A_o} \qquad (4\text{-}2)$$

for the blooming and beam jitter effects considered separately. This is often referred to as the root-sum-squaring (RSS) method for treating the combined beam spreading effects of diffraction, thermal blooming, jitter and turbulence, which implies that all effects are essentially uncoupled or statistically independent and noninteracting. The RSS estimate for $I_{REL}$ is then given by

$$I_{REL}(RSS) = \frac{1}{I_{REL}(B)^{-1} + I_{REL}(J)^{-1} - 1} \quad . \qquad (4\text{-}3)$$

Comparison of values for $I_{REL}(RSS)$ with measured results in Table II shows agreement to within 10% for both the weak and strong blooming cases.

A second, more complete set of results obtained on 4/23 are shown in Figs. 9-13. The cumulative power distribution curves without blooming are shown in Fig. 9 for normalized beam jitter levels of $a_J/a_o$ = 0, 1.15 and 1.72 based on the measured 1/e beam radius $a_f$ of the undistorted beam and the calculated rms beam displacement as determined by the measured rms jitter drive signals and scanner sensitivity. Reductions in average peak irradiance of $I_{REL}$ = 0.5 and 0.36 were observed from visual

averaging of scans of the irradiance profiles with a fast point detector, which corresponds to rms jitter levels of 1.0 and 1.58, respectively. Using the effective area based on the 63% power diameters from Fig. 9 gives the values of $I_{REL}$ = 0.44 and 0.24, respectively, for the two jitter levels.

Cumulative power distribution curves are shown in Figs. 10 and 11 for thermal blooming with and without beam jitter for the power levels of $P_{in}$ = 3, 6.1, 9.5 and 12.1 W, which correspond to the values of the distortion parameter N = 1.3, 2.6, 4.1 and 5.2, respectively. Using the 63% power diameters from Figs. 10 and 11 to define the effective beam areas and relative average irradiances $I_{REL}$ as described above, the normalized average irradiance P $I_{REL}$ versus power P is plotted in Fig. 12 for the different amounts of beam jitter. The dashed lines and open symbols refer to the no blooming case and the decreasing slopes simply reflect the reduced irradiance with increasing beam jitter. Figure 13 shows the normalized, time averaged peak irradiance versus power as determined by the average power collected in a 1 mm diameter aperture centered at the peak. Again, the dashed lines indicate the no blooming case. The trends for the dependence of the peak and average irradiance on power for the different levels of beam jitter correlate very well and exhibit the same crossover at P = 6.1 W for the two jitter levels. The measured values of $I_{REL}$ and $I_{REL}$ (RSS) are given in Table III for the various combinations of blooming strength and beam jitter.

The data on 7/24 was obtained from oscilloscope traces of the beam profile as scanned slowly across a fast detector with a 50 μm diameter aperture. Using the midposition of the irradiance profiles broadened by beam jitter to define the average profile, the peak values were used to define the relative irradiance levels, which are given in Table IV together with the RSS estimates. The normalized average peak irradiance $PI_{REL}$ versus power P is plotted Fig. 14 for the various jitter conditions. As before, the rms jitter levels are nominally 1 and 1.5 times the undistorted beam radius. The data in Fig. 14 shows a trend of decreasing critical (or optimum) irradiance and increasing critical (or optimum) power with increasing beam jitter level. This trend is consistent with what is expected on the basis of simple scaling laws based on the distortion parameter N, as will be discussed further in Section V. The absence of this trend in the data of 4/23 shown in Figs. 12 and 13 is believed to be due to experimental error arising from inaccurately positioning the variable aperture with respect to the peak of the average profile. As mentioned earlier the peak of the average profile was found by nominally moving the aperture across the beam while observing the power meter. Although the power meter response is slow enough (< 1 second) to provide some averaging over the jitter effects the remaining fluctuation tended to cause difficulty in accurately establishing the peak position. The data of 7/24 avoided this difficulty and thus, are believed to be more reliable, since the beam profiles were obtained by scanning the beam across a stationary detector using a slow ramp signal to drive the horizontal mirror scanner. The direction of beam scanning was against the wind tunnel flow and was at a rate corresponding to a velocity of only < 0.03 cm/sec at the focal plane which is negligible compared with the 8 cm/sec flow velocity of the wind tunnel.

In Fig. 15, all of the measured values of relative irradiance for combined jitter and blooming conditions are plotted versus the root-sum-square estimates, $I_{REL}$ (RSS). All of the data lie reasonably close to the 45 degree agreement line which indicates that, within the accuracy limits of the experiment, there is negligible interaction or effect of the wide bandwidth ($\sim$0-150 Hz) beam jitter on thermal blooming. One notable case of rather poor agreement between $I_{REL}$ (meas) and $I_{REL}$ (RSS) in Fig. 15 is seen from Table III to correspond to the case with P=6.1 W or N=2.6 and $a_J/a_o$ = 1.15 from the 4/23 data. Were this value for $I_{REL}$ (meas) to lie on the 45 degree agreement line in Fig. 15, we would have $I_{REL}$ (meas) = 0.25 rather than 0.15. This 67% increase in $I_{REL}$ would increase the average irradiance value in Fig. 12 from 0.9 to 1.5 for P = 6.1 W and the lower jitter level case. This would make the trend of the data similar to that in Fig. 14 and, together with the rather large discrepancy observed in Fig. 15, tends to confirm the suspicion that the measured result for this case is in error.

Regarding error limits for the measurements it is estimated that the absolute accuracy of the data for $I_{REL}$ is approximately $\pm$ 20%. The relative accuracy for the average irradiance versus power data from a particular set taken on the same day is probably much better being on the order of $\pm$ 5%. The major sources of error and estimates of this magnitude are: the laser power level; $\pm$ 2.5%; power meter, $\pm$5%; reading of meter or oscilloscope traces, $\pm$ 2.5%; aperture diameter measurement, $\pm$ 0.25 mm; aperture position exact error uncertain, dependent on amount of jitter and averaging time used; laser mode drifting-potential for large errors but usually can be avoided by monitoring the power level.

## V. MODELING OF BEAM JITTER EFFECTS ON THERMAL BLOOMING

A simple analysis of the implications of the root-sum-square (RSS) hypothesis for treating jitter and blooming effects has been made assuming the simple scaling law to hold (Ref. 15)

$$I_{REL} = \frac{1}{1 + CN^P} \tag{5-1}$$

Here N is the distortion parameter Refs. 4 and 16 and C and p are constants. The focused beam distortion parameter $N \sim 1/\beta$, where $\beta$ can refer to the beam quality factor for the undistorted beam or it can also be used to include the effects of beam jitter and turbulences, i.e.,

$$\beta = \sqrt{1 + (\theta_J/\theta_o)^2 + (\theta_t/\theta_o)^2} \tag{5-2}$$

with $\theta_J$, and $\theta_o$, being the rms jitter and diffraction angles, respectively. Neglecting the turbulence $\theta_t$ spreading, i.e., setting $\theta_t = 0$, the peak intensity with both jitter and blooming effects accounted for is then written

$$\frac{I}{I_o} = \frac{1}{\beta^2} I_{REL}(N) = \frac{1}{\beta^2 + C' \beta^{2-p}} \tag{5-3}$$

with $I_o$ the intensity with no jitter or blooming and $C' = C(N\beta)^p$, which is independent of $\beta$. According to the RSS hypothesis,

$$\frac{I}{I_o} = \frac{1}{1 + (\theta_J/\theta_o)^2 + (\theta_B/\theta_o)^2} = \frac{1}{\beta^2 + \left(\frac{\theta_B}{\theta_D}\right)^2}, \tag{5-4}$$

where $(\theta_B/\theta_D)^2 = (I/I_o)^{-1}_{\beta=1} - 1$ is defined by the blooming loss with no jitter. Using Eq. (5-3) we find that $(\theta_B/\theta_D)^2 = C'$ and thus the RSS hypothesis, Eq. (5-4) becomes

$$\frac{I}{I_o} = \frac{1}{\beta^2 + C'} \tag{5-5}$$

Clearly, for the assumed scaling model Eq. (5-3) to be consistent with the RSS hypothesis Eq. (5-5) or, equivalently, for the beam jitter to not interact with the blooming loss, it follows that the exponent p in Eq.(5-1) must be two. If the experimental data with beam jitter included can be shown to scale with the distortion parameter N, it should be possible to use the model in Eq. (1) to determine the validity of or, the extent of the deviation from, the RSS hypothesis.

It is interesting to note that while the exponent $p^{-2}$ provides a reasonably good fit to both experimental and wave optics code results for Gaussian beam shapes somewhat smaller valves of p are found for uniform and annular beam profiles.

The vertical (or optimum) irradiance and the associated power level for a fixed aperture diameter, range, absorption and velocity conditions has been shown to scale approximately as (Ref. 16),

$$I_c \sim \frac{I}{\beta} \sim \frac{1}{\sqrt{1 + (\theta_J/\theta_o)^2}} \tag{5-6}$$

and

$$P_c \sim \beta \sim \sqrt{C + (\theta_J/\theta_o)^2} \quad , \tag{5-7}$$

respectively. Thus, beam jitter decreases the critical (or optimum) irradiance and increases the critical (or optimum) power by the same factor $\beta$. Using the 4/24 data shown in Fig. 14 the scaling of the measured critical irradiance and power levels for the two jitter levels of $a_J/a_o = 0.9$ and 1.4 is compared with the scaling based on Eqs.(5-6 and 5-7). The results which are shown in Table V, indicate the prediction of the scaling expression for the critical irradiance is about 15% greater than the measured results. The measured values of critical power are 23% below and about 10% greater than the scaling law predictions for the small and larger jitter levels, respectively. Although the agreement between the scaling law predictions and the measurements could be better at least there is agreement in the

gross dependence on beam jitter level. Since the scaling expressions have been derived assuming weak absorption, or with $\alpha z \ll 1$, it is possible that an improved expression could be obtained by taking into account the effect of finite $\alpha z$ where determining the correction factor to account for focusing in the distortion parameter N. It is through the dependence of N on the degree of focusing that the effects of beam jitter as well as poor beam quality and turbulence are accounted for in predicting the thermal distortion effects.

## VI. FUTURE PLANS

During the remainder of the contract period the experimental measurements and analysis of beam jitter effects on thermal blooming will be continued. Although some additional broadband, jitter data remains to be analyzed, the emphasis in the experimental effort will be to examine the dependence of the jitter effects on blooming or the ratio of jitter frequency to the blooming frequency, $f_J/f_B$. Thus, narrow band, tunable random jitter signals at frequencies less than, comparable to, and larger than the blooming frequency defined at the focus will be used to determine the frequency dependence of the jitter effects on blooming. Data will be obtained showing the effects of the various beam jitter frequencies on the focal plane irradiance versus power curve. The experimental results for $I_{REL}$ will be compared to estimates based on the root-sum-square approach. In addition, efforts will be continued to check the experimental results against existing scaling relations and, if necessary, attempt to determine appropriate modifications. Further efforts will be made to more accurately assess and to reduce the errors associated with the blooming experiments. In particular, laser power will be monitored with a strip chart recorder and the irradiance profiles will be measured by automatically scanning the beam rather than using the variable aperture approach to improve the accuracy and repeatability of the experimental results.

REFERENCES


1. F. G. Gebhardt and D. C. Smith, Appl. Phys. Lett. 14, 52 (1969).

2. D. C. Smith and F. G. Gebhardt, Appl. Phys. Lett. 16, 275 (1970).

3. F. G. Gebhardt and D. C. Smith, IEEE J. Quantum Electron QE-7, 63 (1971).

4. _____, Annual Reports on Army Contract DAAB07-70-C-0204 with U. S. Army ECOM for the periods 30 April 1970 to 29 April 1971 (AD905633) and 30 April 1971 to 20 April 1972 (AD765520).

5. _____, Appl. Optics 11, 244 (1972).

6. R. J. Hull, P. L. Kelly and R. L. Carman, Appl. Phys. Lett. 17. 539, (1970).

7. J. Wallace and M. Camac, J. Opt. Soc. Am. 60, 1587 (1970).

8. P. N. Livingston, Appl. Optics, 10, 426 (1971).

9. L. C. Bradley and J. Herrmann, J. Opt. Soc. Am. 61, 668 (1971).

10. J. N. Hayes, P. B. Ulrich and A. H. Aitken, Appl. Optics 11, 257 (1972); P. B. Ulrich, J. N. Hayes and A. H. Aitken, J. Opt. Soc. Am. 62, 298 (1972).

11. J. A. Fleck, Jr. and J. R. Morris, "Recent Four-D Calculations of Time Dependent Propagation Phenomena" (U), First Do D Conference on High Energy Laser Technology, October 1974, San Diego, Calif. (SECRET-NOFORN)

12. T. R. Welch, Airborne Pointing and Tracking Systems, (U), Technical Report (Draft), P72-188, Contract F29601-72-C-0029, Hughes Aircraft Company, Culoer City, California, June 1972 (SECRET-NOFORN).

13. The accuracy of the flowmeter is this low velocity range is quoted by the manufacturer as ±2% + 5cm/sec. Subsequently, calibration by mechanically scanning the hot wire probe at a known velocity has been used to establish the minimum usable velocity of the wind tunnel at about 2 cm/sec.

14. P. J. Berger, F. G. Gebhardt and D. C. Smith, "Thermal Blooming Due to a Stagnation Zone in a Slewed Beam," Final Technical Report on Contract N00014-73-C-0454, October 15, 1974, United Aircraft Research Laboratories Report N921724-12.

15. This form for $I_{REL}$ has been found to provide a reasonably good fit to both experimental and numerical thermal blooming data, (e.g., the values of $C = 0.0895$ and $p = 1.22$ are found for the uniform beam shape results in Fig. 5 of Ref. 16).

16. F. G. Gebhardt, "Effect of Aperture Diameter on cw Thermal Blooming," United Aircraft Research Laboratories Report, UAR-N182, December 1974.

17. _____, "Review of High Power Propagation," present at May 1975 IEEE/OSA Conference on Laser Engineering and Applications. (Submitted for publication in Applied Optics). United Technologies Research Center Report UTRC75-38, July 1975.

TABLE I

EXPERIMENTAL PARAMETERS

Absorbing Medium:

air + propylene ($C_3H_6$) at 1 atm pressure

$\alpha t$ = 1.55 (4/11), 1.24 (4/23), 0.66 (4/24)

v = 0 cm/sec (wind tunnel velocity)

Distances:

absorbing pathlength t = 99 cm

cell input to detector pinhole z = 104 cm

focal range F = z

vertical (y) scanner mirror to detector = 115 cm

horizontal (x) to vertical (y) scanners = 5 cm

X - Y Mirror Scanners:

sensitivity = 0.17 mrad/mv

jitter signals = 0, 3 & 4.5 mv rms (wide band noise ~ 0-300 Hz)

Laser:

$CO_2$ at 10.6 $\mu$ wavelength

$a_i$ = 0.36 cm (i/e radius at cell input)

$a_o$ = 0.066 cm (i/e radius in focal plane)

## Table II

### Relative Irradiances (4/11 Data)

| N ($P_{in}$) | $I_{REL}$ (Measured)* $a_J/a_o = 0$ | $I_{REL}$ (Measured)* $a_J/a_o = 0.94$** | $I_{REL}$ (RSS) $a_J/a_o = 0.94$** |
|---|---|---|---|
| 0 | 1.0 | 0.53 | 0.53 |
| 2.9 (5.5) | 0.46 | 0.32 | 0.33 |
| 5.8 (11) | 0.094 | 0.096 | 0.087 |

*$I_{REL}$ (Measured)= $(d_{eo}/d_e)^2$ where $d_{eo}$, $d_e$ are the 63% power diameters measured for the ideal (unjittered and unbloomed) and distorted and/or jittered beams, respectively. $I_{REL}$ (RSS) is defined in Eq. (4-3).

**Here the normalized jitter radius $a_J/a_o$ is defined in terms of $I_{REL}$ based on the 63% power diameters.

TABLE III

RELATIVE IRRADIANCES (4/23 DATA)

| N (Pin) | $*I_{REL}$ (Measured) $a_J/a_o=0$ | 1.13 | 1.78 | $I_{REL}$ (RSS) 1.13 | 1.78 |
|---|---|---|---|---|---|
| 0 | 1.0 | 0.44 | 0.24 | | |
| 1.3 (3) | 0.5 | 0.30 | 0.18 | 0.305 | 0.19 |
| 2.6 (6.1) | 0.38 | 0.15 | 0.15 | 0.26 | 0.17 |
| 4.1 (9.5) | 0.12 | 0.09 | 0.12 | 0.10 | 0.09 |
| 5.2 (12.1) | 0.06 | 0.03 | 0.04 | 0.05 | 0.05 |

$*I_{REL}$(Measured) is as deformed in Table II and $I_{REL}$ (RSS) as in Eq. (4-3).

TABLE IV

RELATIVE IRRADIANCES (4/24 DATA)

| | $*I_{REL}$ (Measured) | | | $I_{REL}$ (RSS) | |
|---|---|---|---|---|---|
| N (Pin) | $a_J/a_o$=0 | 0.9 | 1.4 | 0.9 | 1.4 |
| 0 | 1.0 | 0.56 | 0.34 | | |
| 0.9 (3) | 0.88 | 0.51 | 0.37 | 0.52 | 0.32 |
| 1.7 (6) | 0.65 | 0.39 | 0.28 | 0.43 | 0.29 |
| 2.6 (9) | 0.36 | 0.29 | 0.21 | 0.28 | 0.21 |
| 3.5 (12) | 0.29 | 0.19 | 0.16 | 0.23 | 0.18 |
| 4.3 (15) | 0.16 | 0.15 | 0.14 | 0.14 | 0.12 |

*$I_{REL}$ (Measured) is based on the peak values of the time averaged irradiance profiles. $I_{REL}$ (RSS) is defined in Eq. (4-3).

TABLE V

CRITICAL IRRADIANCE AND POWER SCALING
WITH BEAM JITTER (4/24 DATA)

| | $I_c(J)/I_{co}$ | | $P_c(J)/P_{co}$ | |
|---|---|---|---|---|
| $a_J/a_o$ | Measured | Eq. (5-6) | Measured | Eq. (5-7) |
| 0.9 | 0.65 | 0.74 | 1.1 | 1.35 |
| 1.4 | 0.51 | 0.58 | 1.9 | 1.72 |

$I_{co}$ and $P_{co}$ are the critical irradiance and power, respectively, without beam jitter.

# LIST OF FIGURES

# BEAM JITTER SPECTRUM

RMS JITTER ~15 μRADIANS

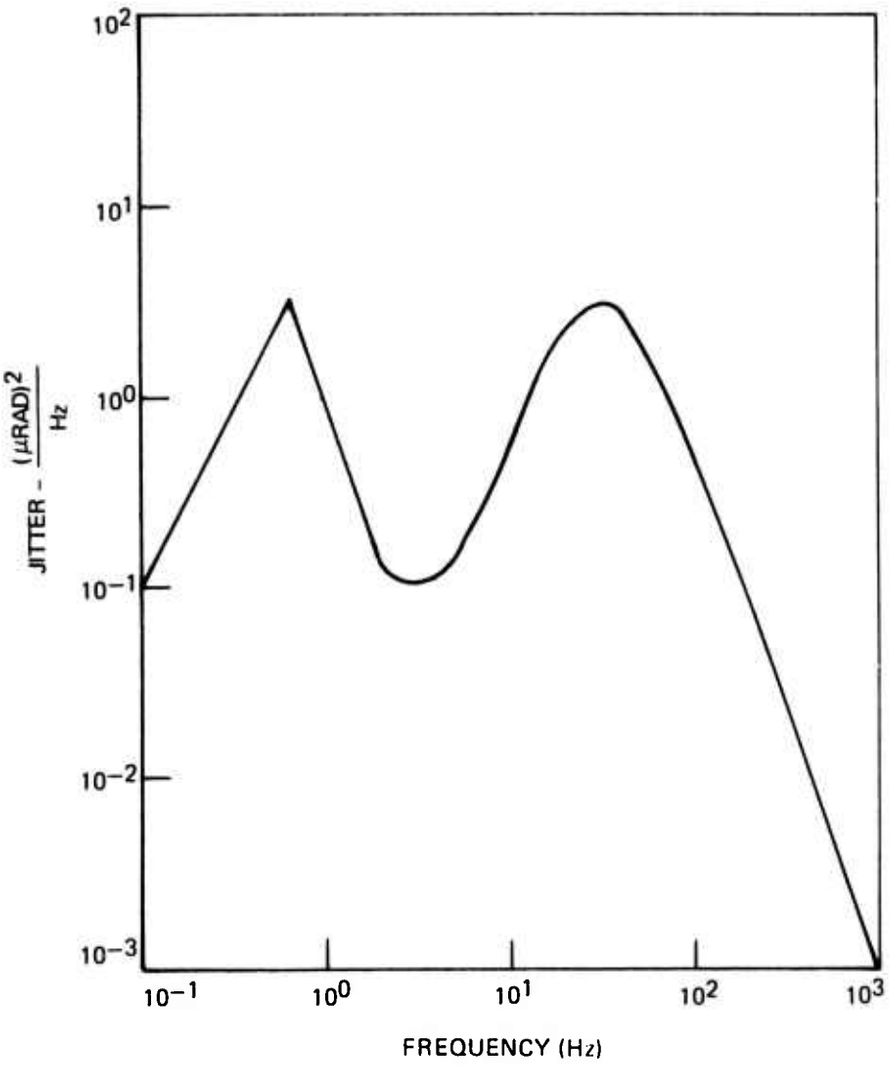

FIG. 2

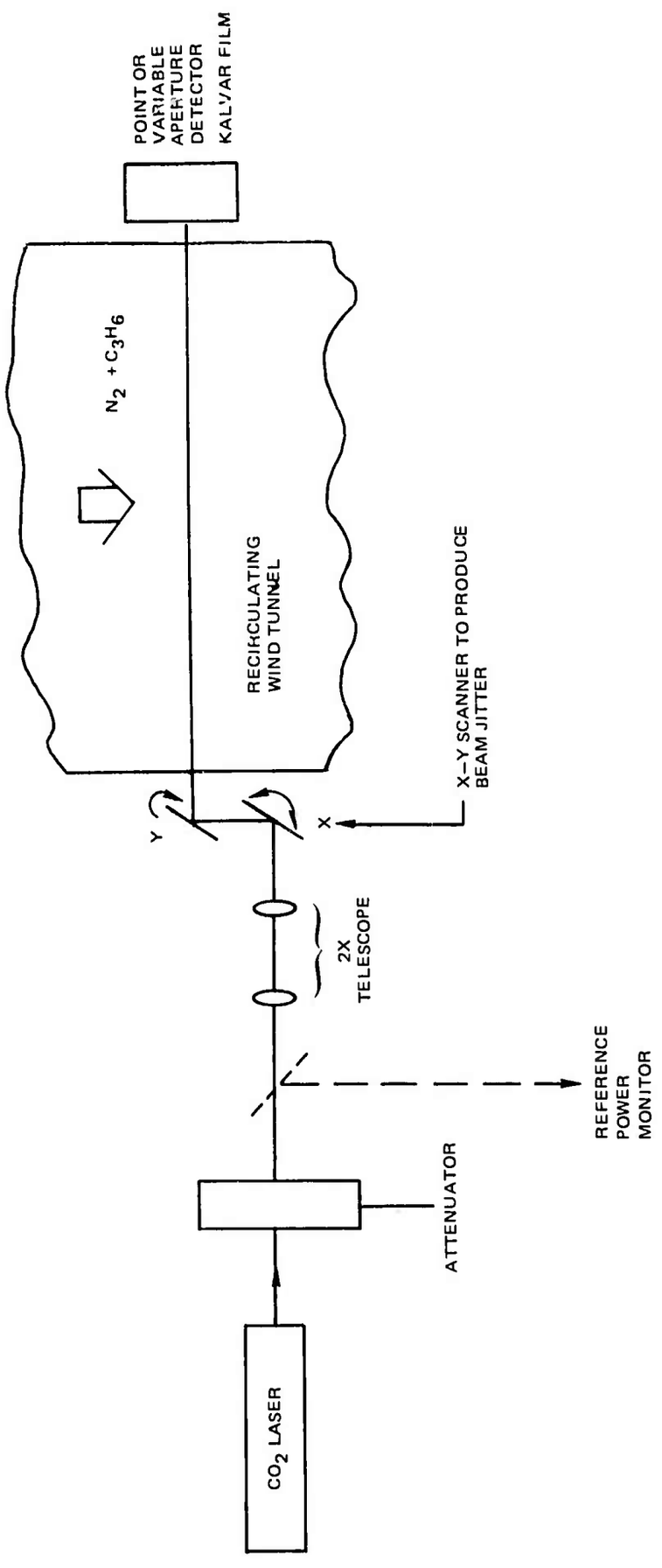


EXPERIMENTAL ARRANGEMENT

R06-252-9

FIG. 3

## MEASURED FREQUENCY RESPONSE OF G-300 PD GALVONOMETER SCANNERS

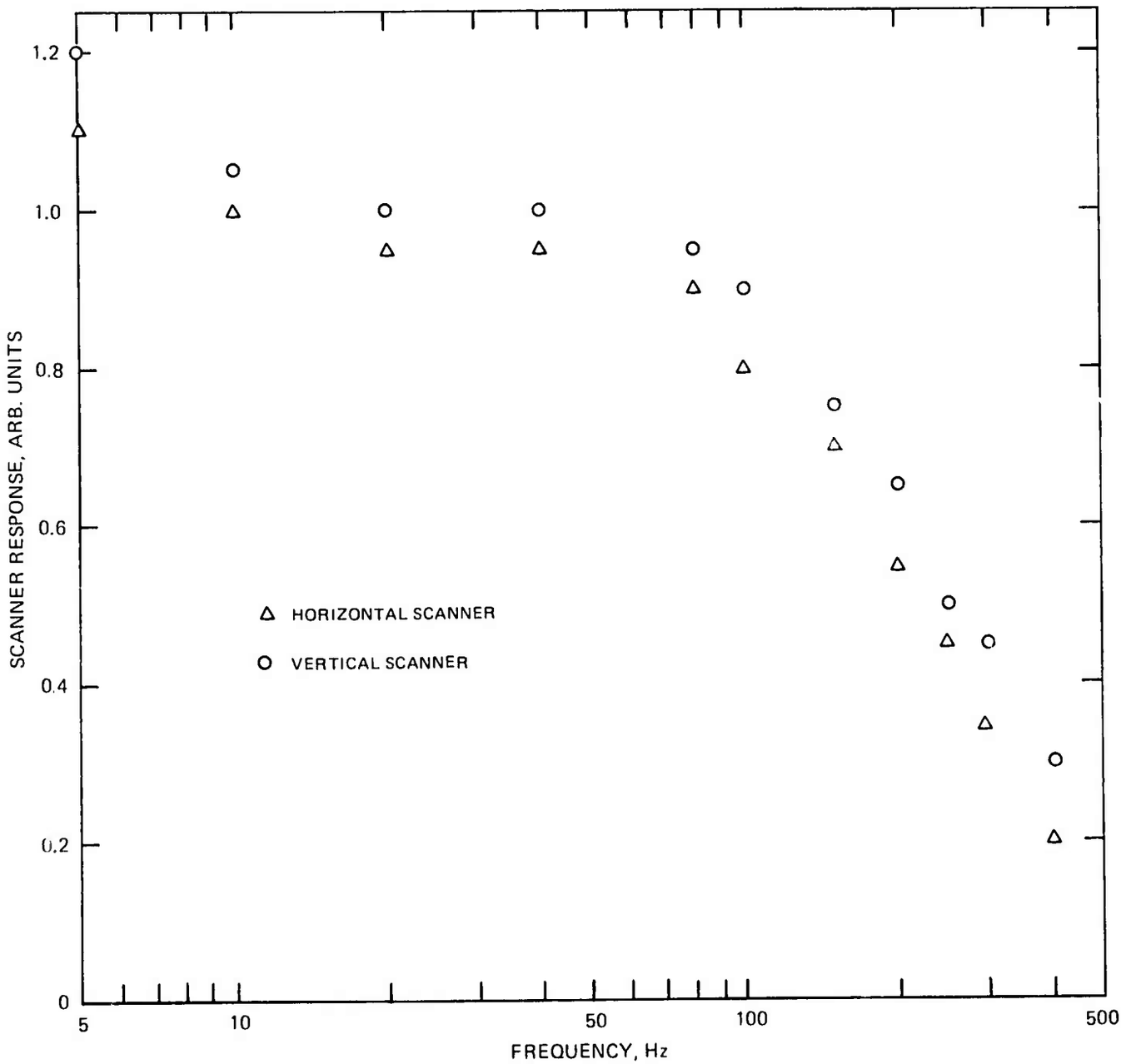

FIG. 4

## BEAM JITTER DRIVE SIGNAL SOURCE

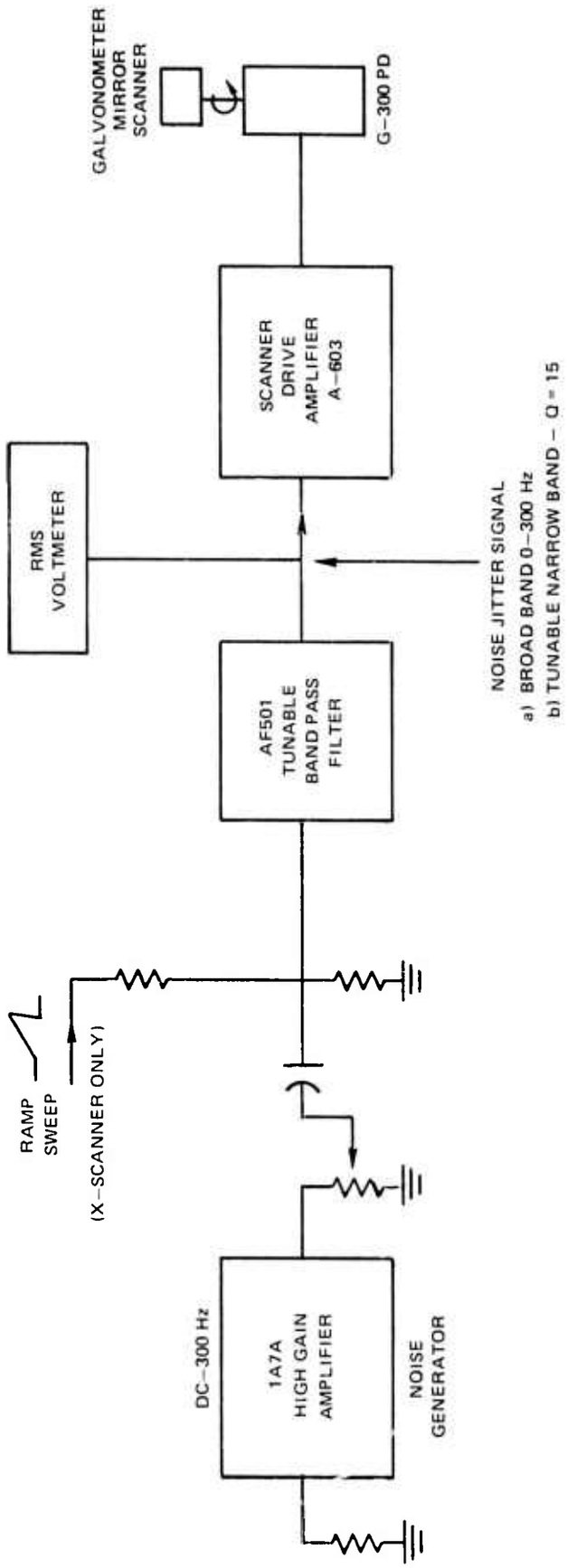

## INPUT BEAM INTENSITY PATTERN AND PROFILE

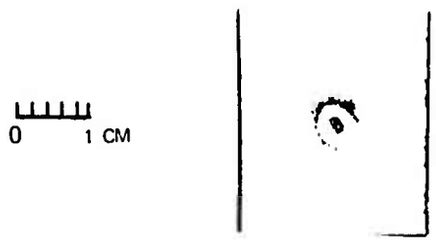


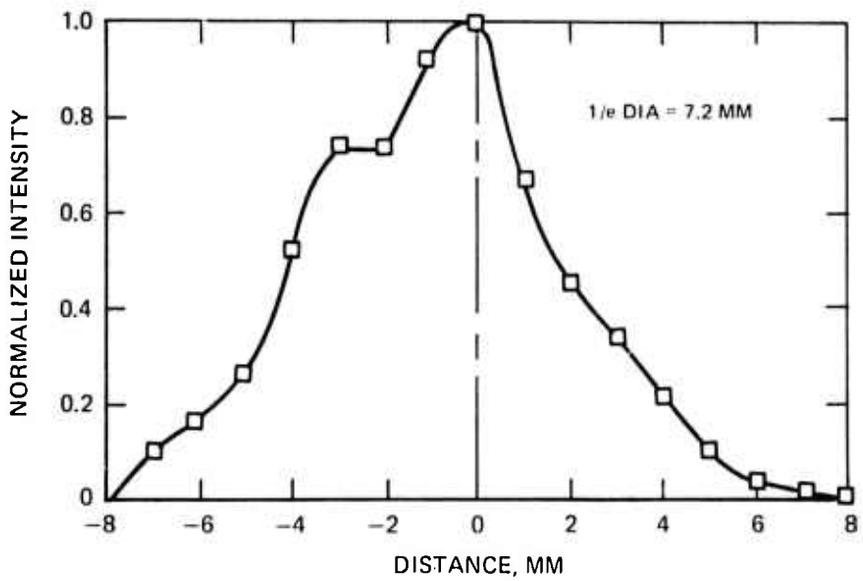

# MEASURED BEAM PATTERNS AND PROFILES
# (NO THERMAL BLOOMING)

W/O JITTER

VERTICAL SCALE: 2 V/DIV
HORIZONTAL SCALE: 0.75 mm/div
SWEEP RATE: 0.5 sec/div

W/JITTER
$a_J(\text{RMS}) = 1.15\, a_o$
BANDWIDTH: 0–300 Hz

0 1 CM

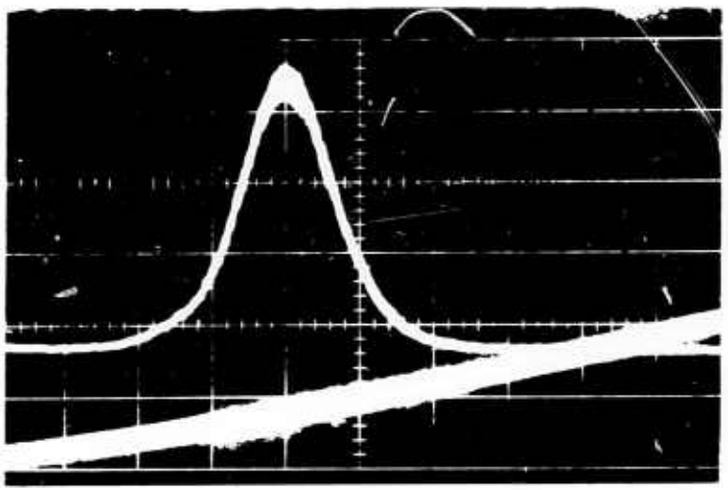

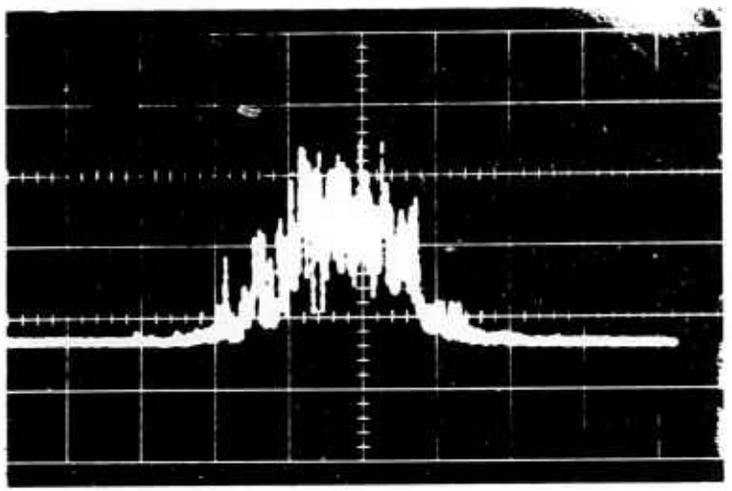





FIG. 6

FIG. 7

## CUMULATIVE POWER DISTRIBUTION

W/O BLOOMING

○ W/O JITTER

△ W/JITTER

W/BLOOMING $P_{in}$ = 5.5W

● W/O JITTER

▲ W/JITTER

NORMALIZED RMS JITTER: $a_J/a_o$ = 1.15

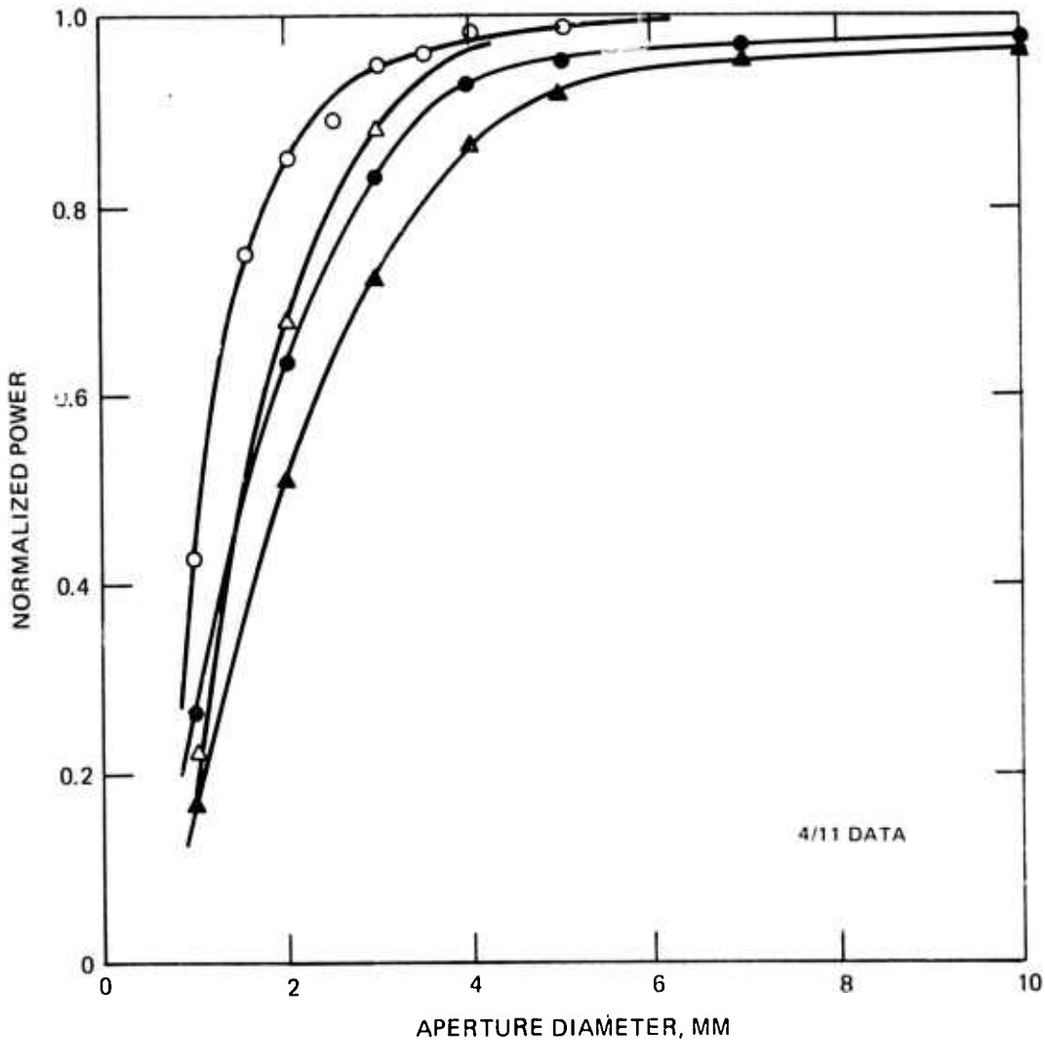

FIG. 8

## CUMULATIVE POWER DISTRIBUTION

W/O BLOOMING.

○ W/O JITTER

△ W/JITTER

W/BLOOMING $P_{in}$ = 11 W

● W/O JITTER

▲ W/JITTER

NORMALIZED RMS JITTER: $a_J/a_O$ = 1.15

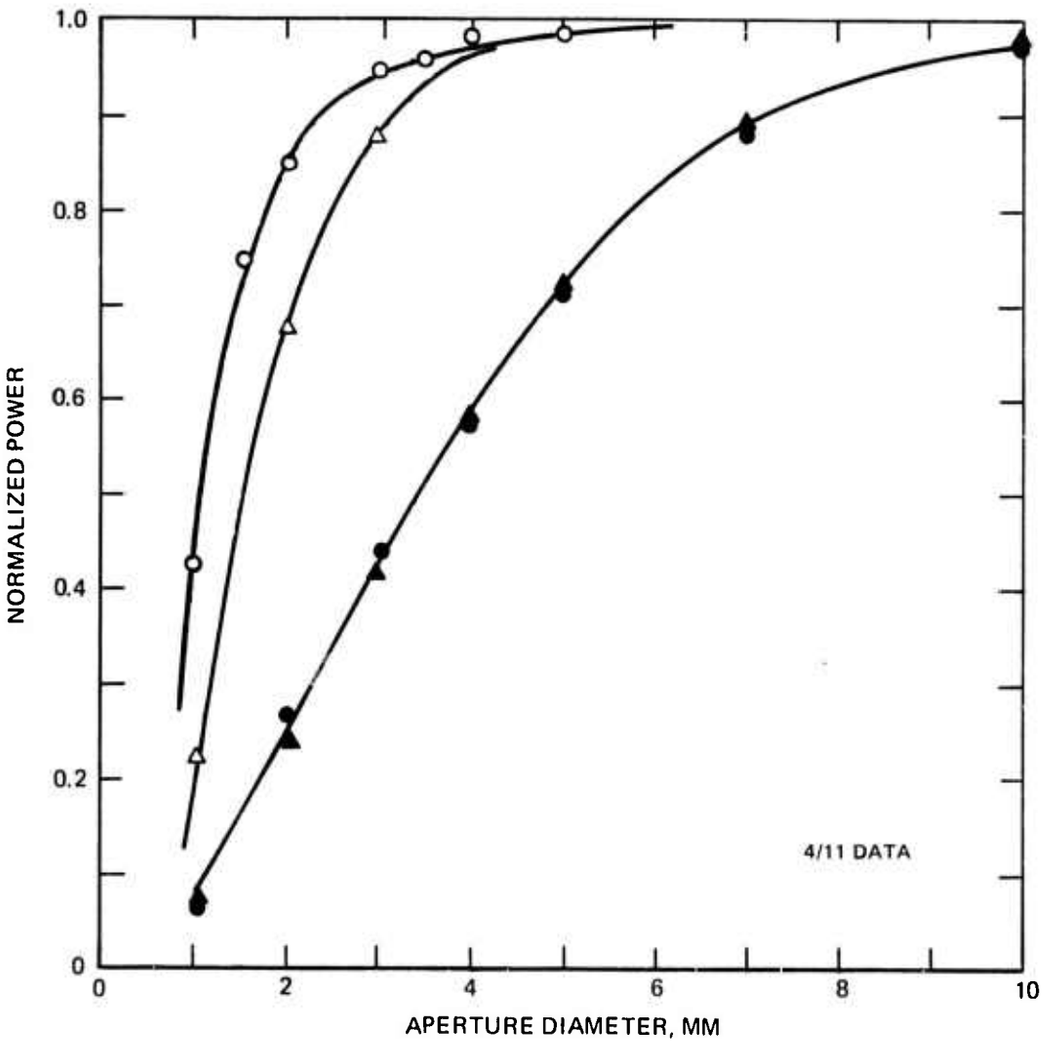

FIG. 9

## CUMULATIVE POWER DISTRIBUTION

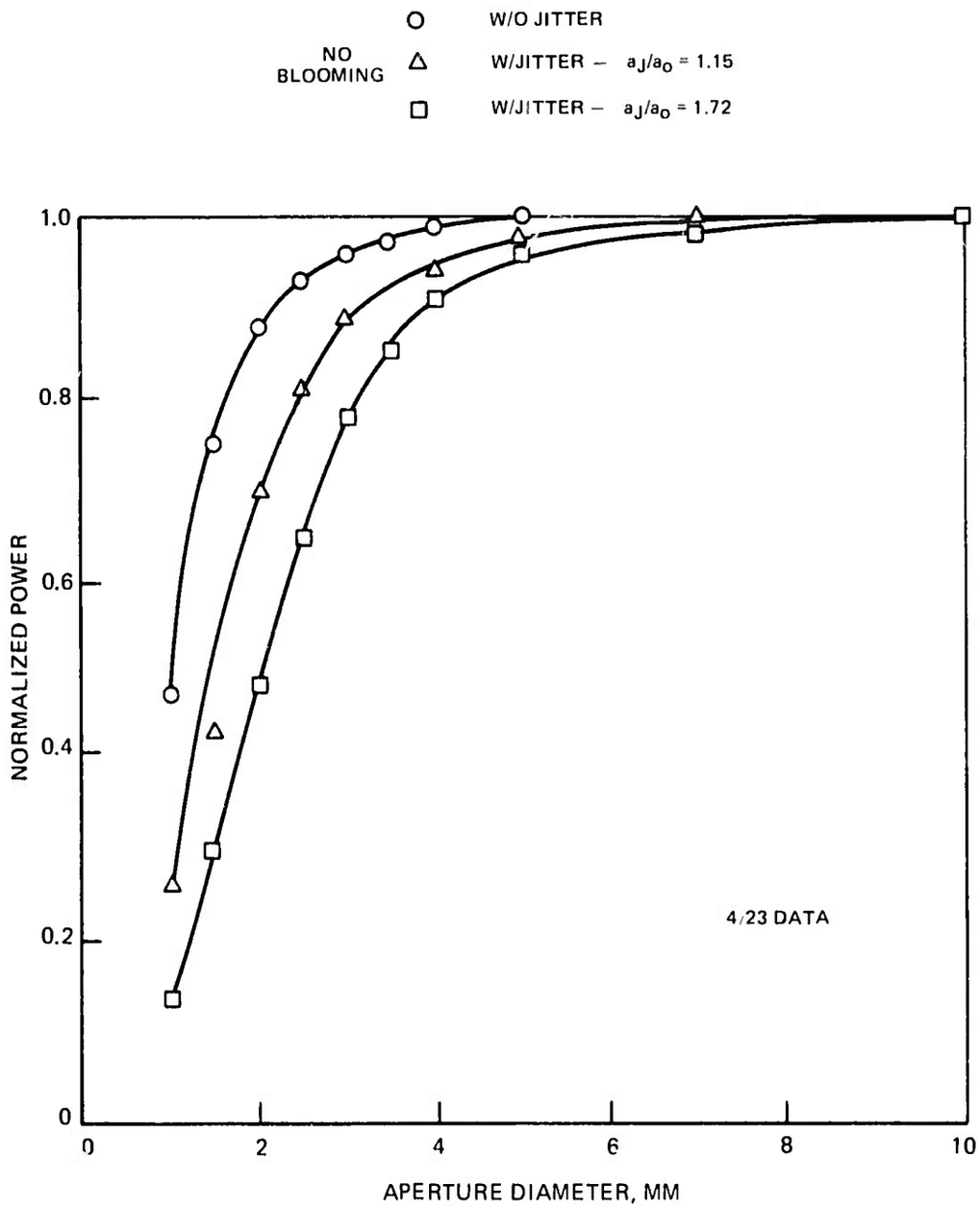




R07–147–1

## CUMULATIVE POWER DISTRIBUTION

- ● W/O JITTER
- ▲ W/JITTER – $a_J/a_O$ = 1.15
- ■ W/JITTER – $a_J/a_O$ = 1.72

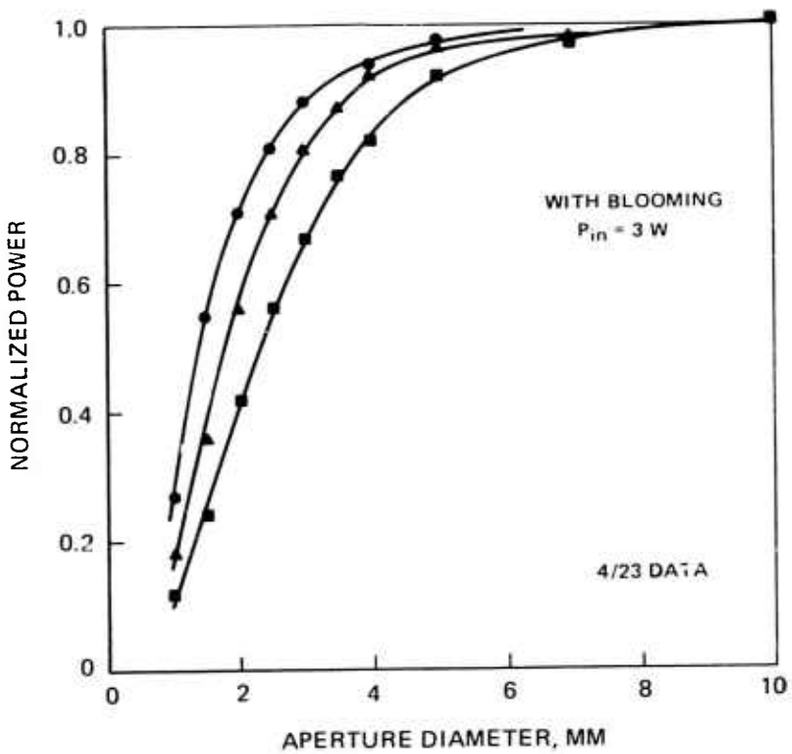


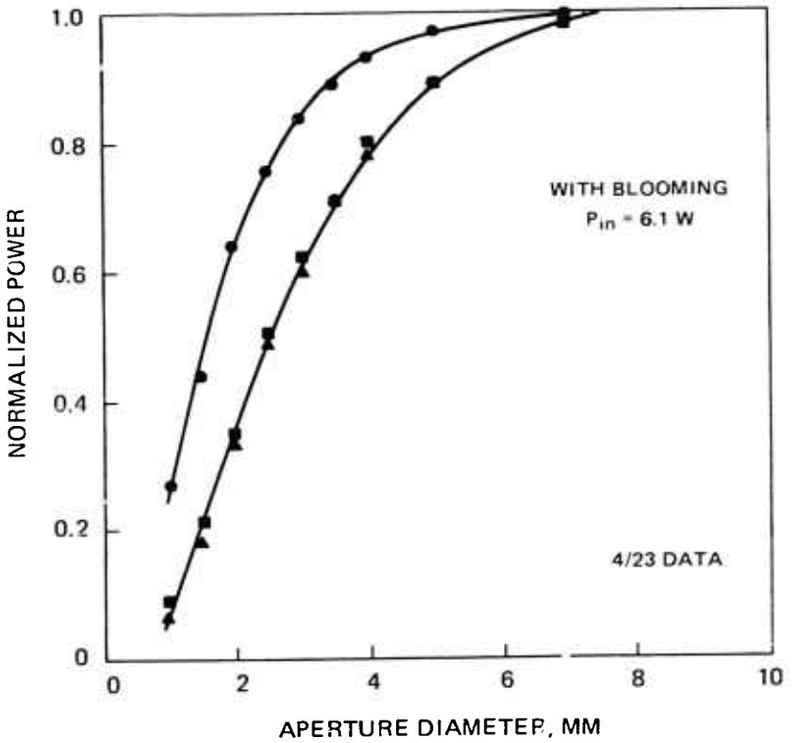


FIG. 10

FIG. 11

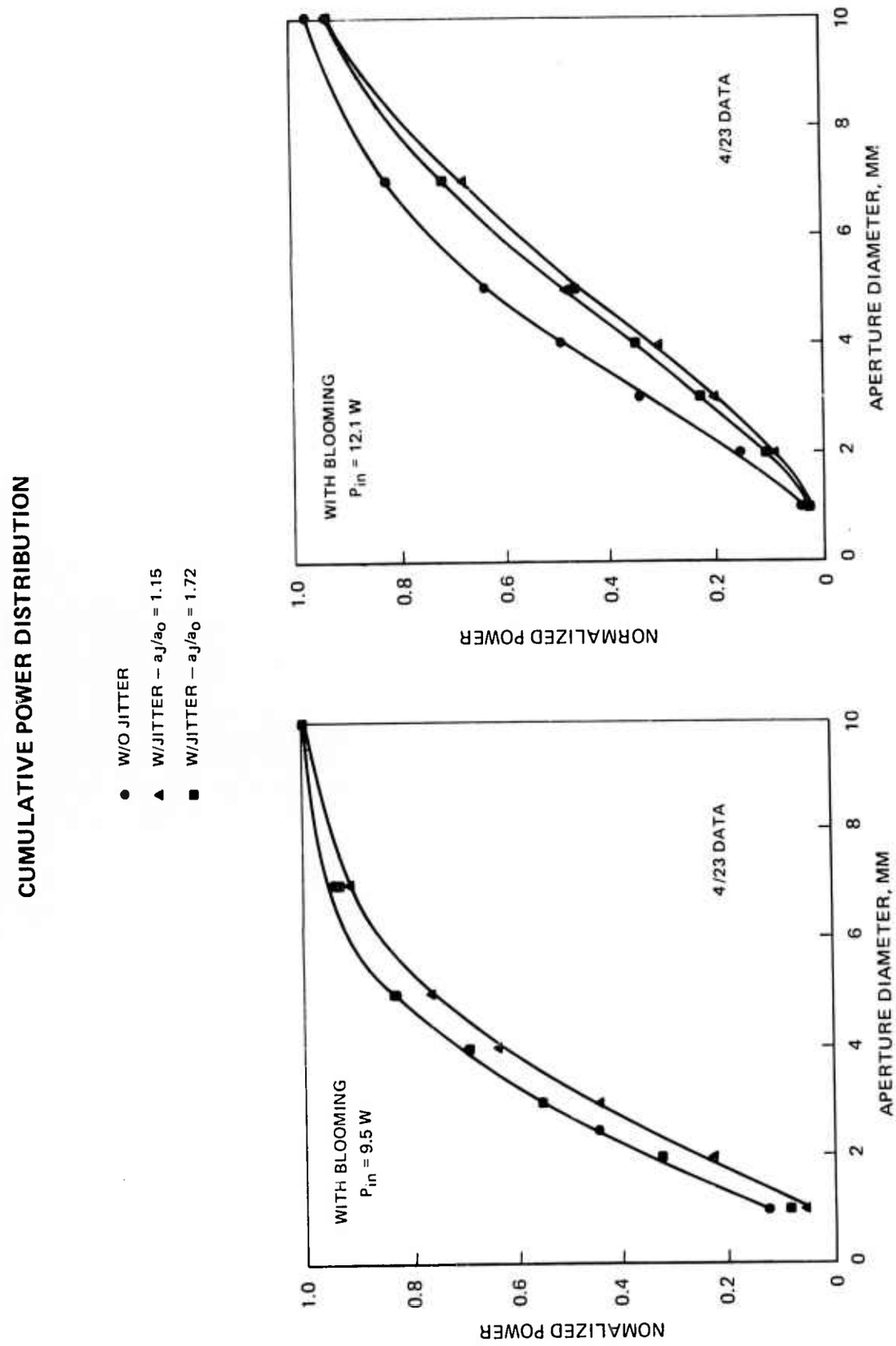
CUMULATIVE POWER DISTRIBUTION
● W/O JITTER
▲ W/JITTER – $a_J/a_O$ = 1.15
■ W/JITTER – $a_J/a_O$ = 1.72
WITH BLOOMING
$P_{in}$ = 12.1 W
4/23 DATA
NORMALIZED POWER
APERTURE DIAMETER, MM
WITH BLOOMING
$P_{in}$ = 9.5 W
4/23 DATA
NORMALIZED POWER
APERTURE DIAMETER, MM

FIG. 12

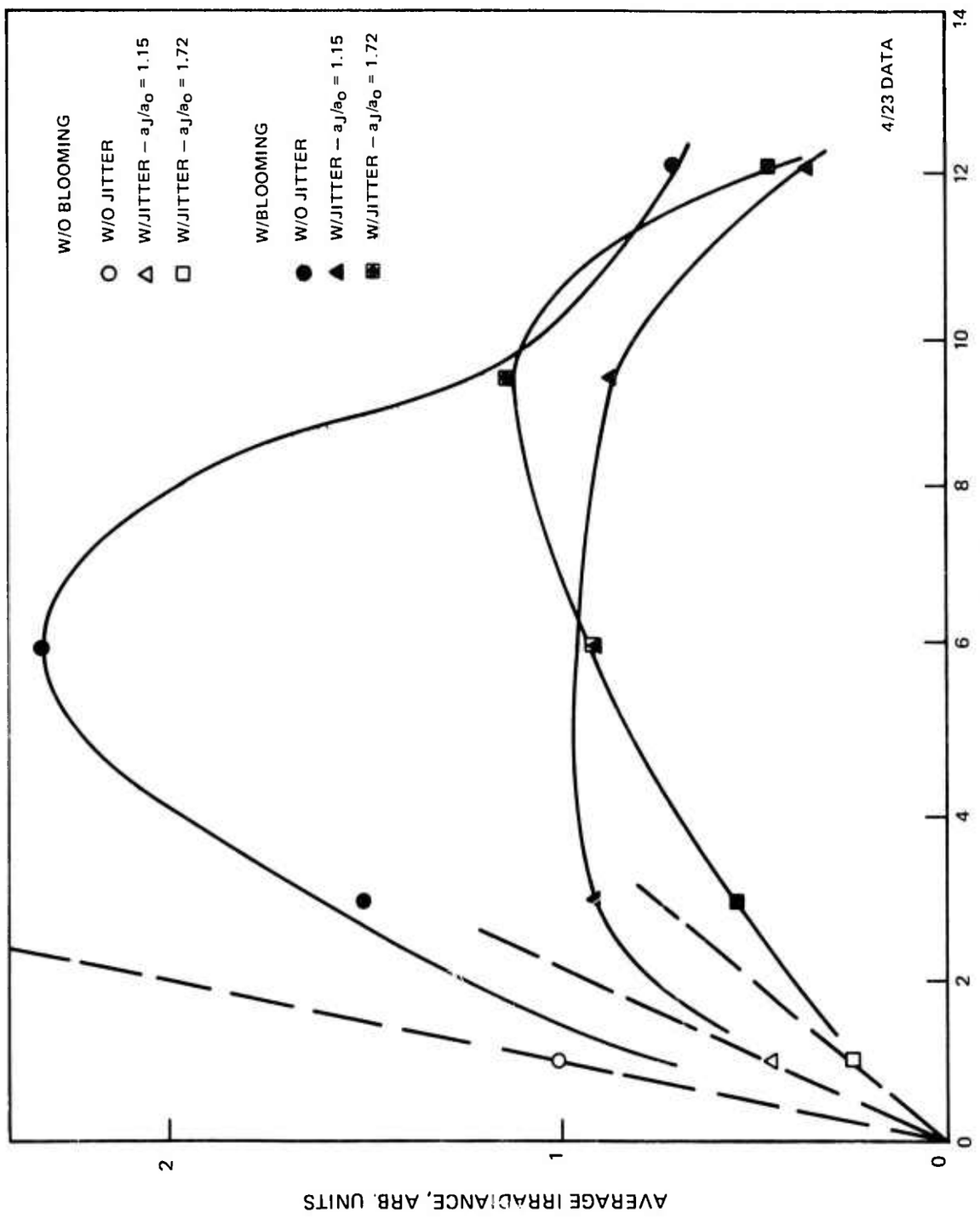


R07–147–4

FIG. 13

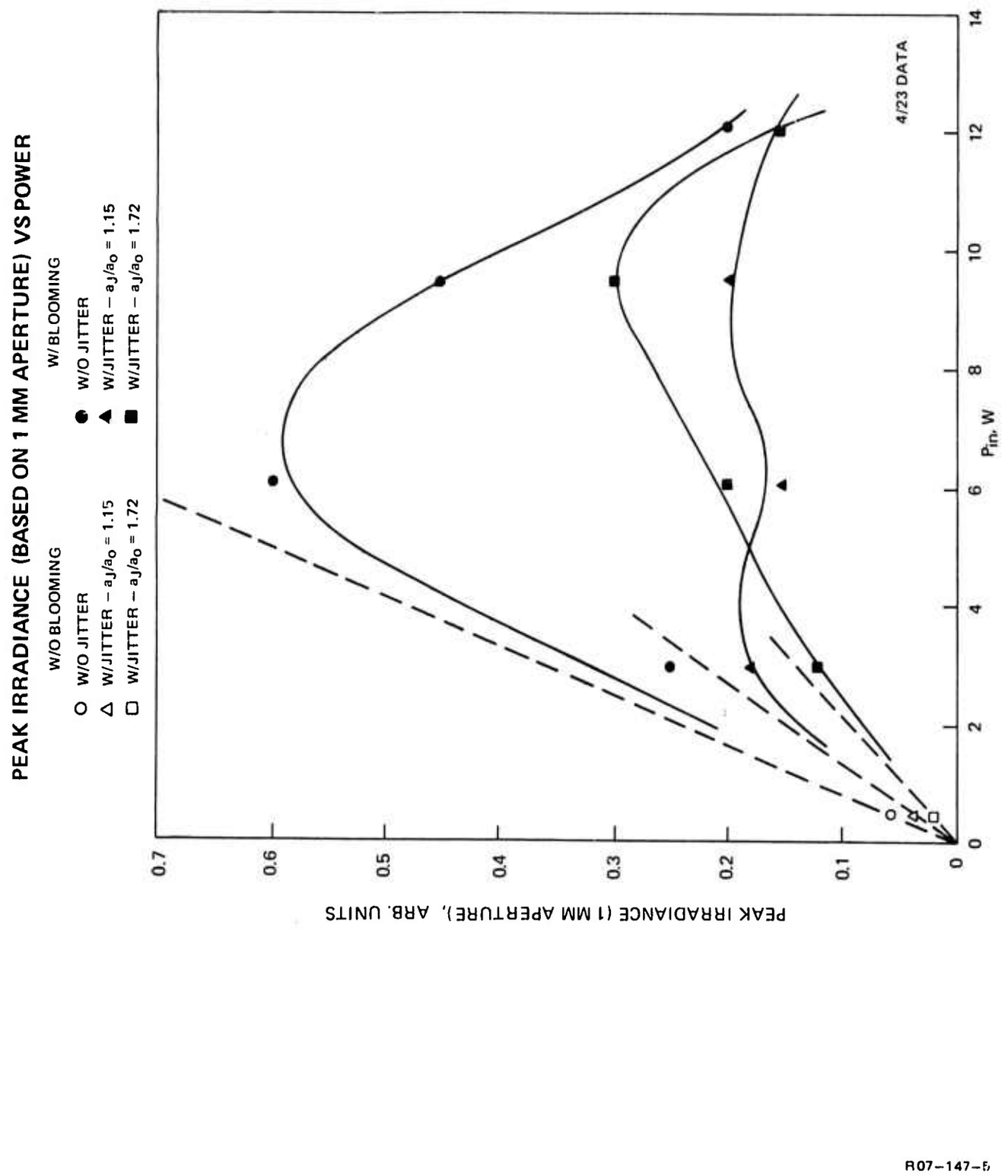




R07-147-5

FIG. 14

PEAK IRRADIANCE (BASED ON AVERAGE BEAM PROFILE) VS POWER

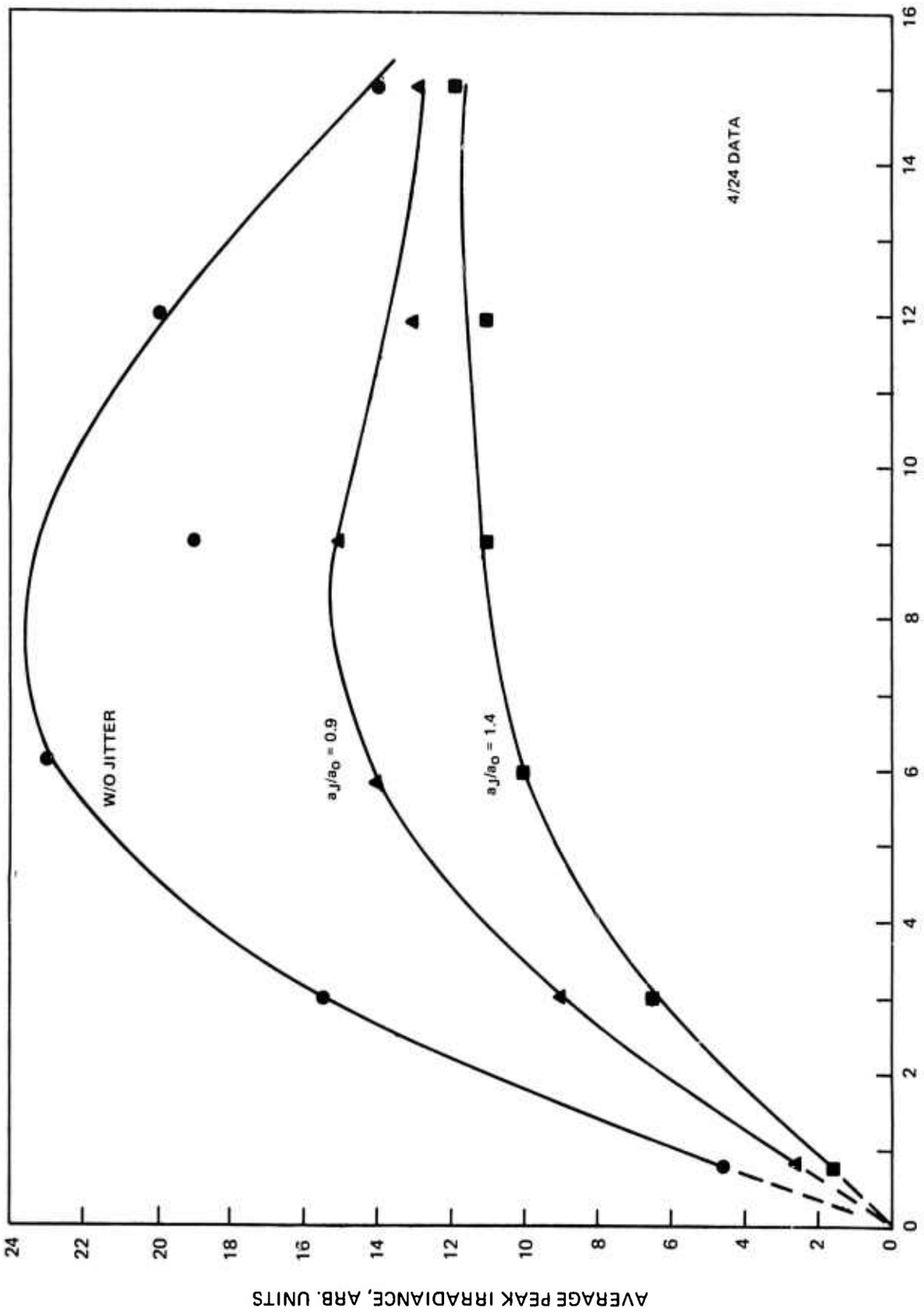


39

807–147–6

FIG. 15

## MEASURED VS ROOT–SUM–SQUARE RESULTS FOR BEAM JITTER AND BLOOMING

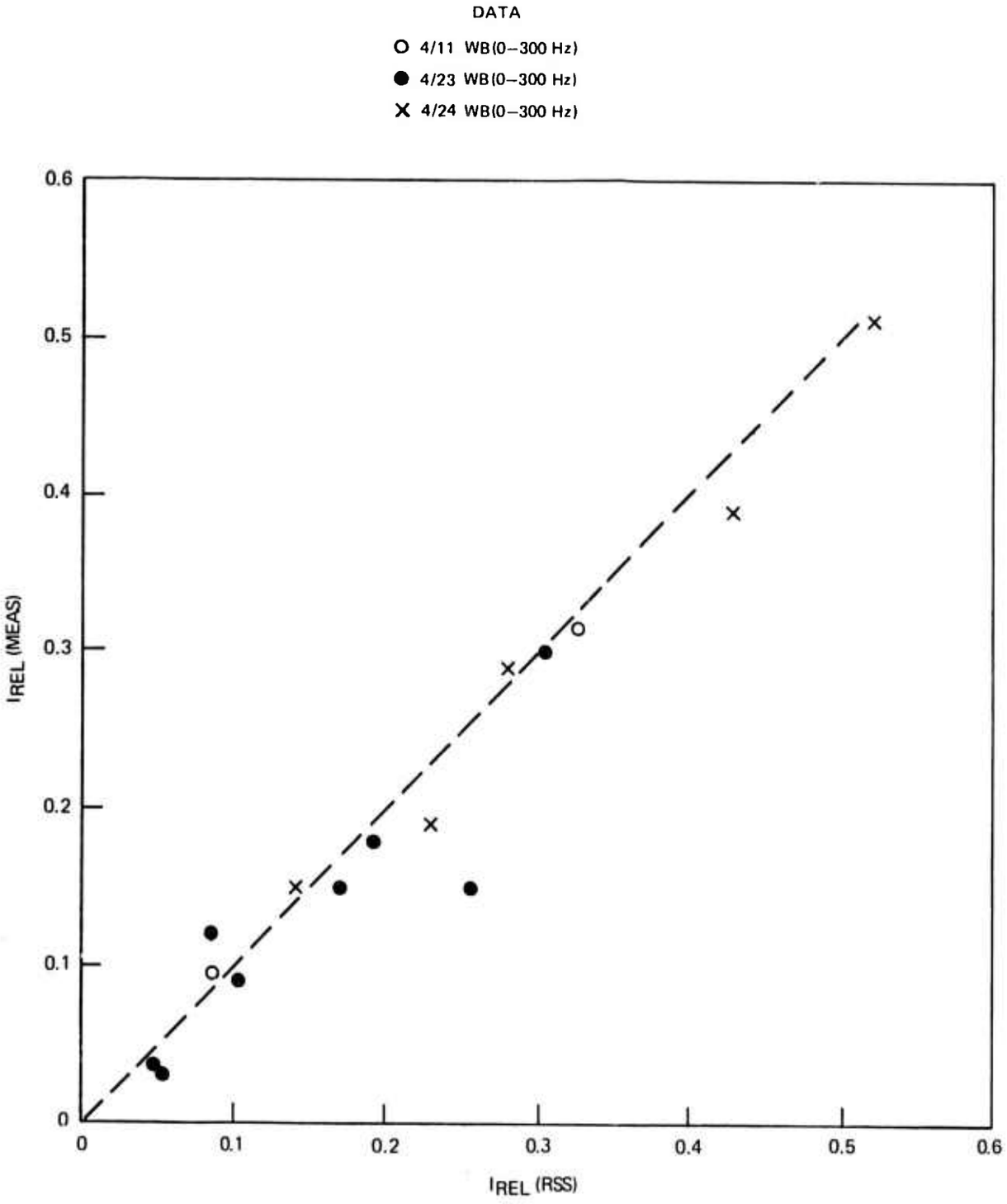




R07–147–7